BIOCHEMISTRY
including biophysical chemistry & molecular biology

Article

pubs.acs.org/biochemistry

Manipulating Cofactor Binding Thermodynamics in an Artificial Oxygen Transport Protein

Lei Zhang,[†] J. L. Ross Anderson,[‡,∥] Ismail Ahmed,[†] Jessica A. Norman,[†] Christopher Negron,[†,§] Andrew C. Mutter,[†] P. Leslie Dutton,[‡] and Ronald L. Koder*[,†]

[†]Department of Physics, The City College of New York, New York, New York 10031, United States

[‡]Department of Biochemistry and Biophysics, The University of Pennsylvania School of Medicine, Philadelphia, Pennsylvania 19104, United States

ABSTRACT: We report the mutational analysis of an artificial oxygen transport protein, HP7, which operates via a mechanism akin to that of human neuroglobin and cytoglobin. This protein destabilizes one of two heme-ligating histidine residues by coupling histidine side chain ligation with the burial of three charged glutamate residues on the same helix. Replacement of these glutamate residues with alanine, which is uncharged, increases the affinity of the distal histidine ligand by a factor of 13. Paradoxically, it also decreases heme binding affinity by a factor of 5 in the reduced state and 60 in the oxidized state. Application of a three-state binding model, in which an initial pentacoordinate binding event is followed by a protein conformational change to hexacoordinate, provides insight into the mechanism of this seemingly counterintuitive result: the initial pentacoordinate encounter complex is significantly destabilized by the loss of the glutamate side chains, and the increased affinity for the distal histidine only partially compensates for that. These results point to the importance of considering each oxidation and conformational state in the design of functional artificial proteins.

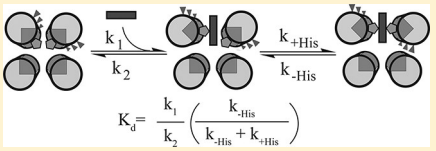

Designed proteins containing bound cofactors, both natural and synthetic, hold great promise as inexpensive biocompatible catalysts useful in medicine, energy production, and green industrial catalysis.[1−3] Heme proteins were the first bioinorganic cofactor-containing proteins created more than 15 years ago,[4,5] and since then, they have proven to be instructive with respect to the underlying engineering requirements that drive natural heme protein evolution.[6−8]

Members of the family of hexacoordinate hemoglobins are characterized by the property that they are bis-histidine-ligated in the oxidized state and exist in a mixed bis- and monohistidine ligation state when reduced.[9] The transient pentacoordination of the heme cofactor allows for the ligation of molecular oxygen. We have recently reported the design, bacterial expression, and biochemical analysis of the completely artificial hexacoordinate oxygen transport protein HP7.[10] This was the culmination of a series of design projects involving helical bundles that bind heme.[11−16] Homodimeric protein HP7 is composed of two helix−loop−helix peptides in which the loops connect via a disulfide in a topology we have termed the "candelabra" motif[12] (see Figure 1A, sequences in Figure 1E).

HP7 and its progenitors were designed in part using the principles of binary patterning, a simple alternating pattern of hydrophilic and hydrophobic helix-forming residues with the heptamer repeat sequence ●○○●●○○, where the first, third, and fourth amino acids are nonpolar (●) and the rest are polar (○) (see Figure 1E), which imposes dimerization via hydrophobic sequestration.[17−21] Each residue in the heptad repeat is designated with a letter; thus, the hydrophobic residues are at positions a, d, and e of the heptad. There is a histidine residue at position 6 of each helix, positioned to lie at position a of the heptad repeat.[13] Two heme cofactors bind, one between each matching pair of histidines in the homodimer, and each binding event induces a large-scale helical rotation that brings three b-position glutamate residues into the hydrophobic core of the protein. The burial of these residues creates an "entatic" state:[22] this stored energy is utilized to drive the detachment of the ligand histidine residue from that helix, allowing the subsequent rotation of the helix to a relaxed state in which these b-position side chains are exposed to solvent, opening a coordination site for the ligation of the gaseous ligands oxygen and carbon monoxide (Figure 1B−D).[10] This design exercise turned out to be instructive with respect to the minimal engineering requirements for oxygen transport, a porphyrin cofactor with an at least transiently pentacoordinate ferrous iron buried within a hydrophobic cavity sufficiently large and stable to restrict water penetration.[11]

Thus, in HP7 as well as the natural hexacoordinate hemoglobins, gaseous ligand affinity is gated by the presence of the pentacoordinate state. Many enzymes, especially those that utilize molecular oxygen as a substrate, contain a number of redox active cofactors in addition to the active site heme. These other cofactors, for example, the heme cofactors in the cytochrome *c* oxidase, typically serve to ferry electrons into the O_2-utilizing active site.[23] These enzymes restrict oxygen binding at the other heme cofactors by maintaining them in the hexacoordinate state. Therefore, it will prove to be important,

Received: August 8, 2011
Revised: October 14, 2011
Published: October 17, 2011

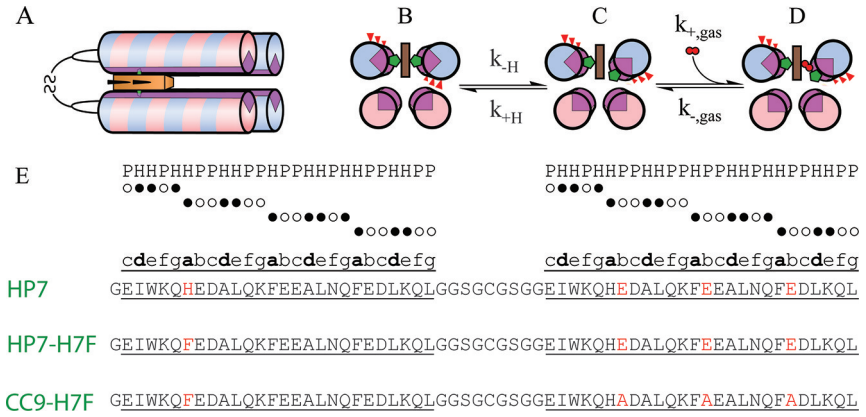

Figure 1. Structure, sequence, and mechanism of HP7 and its mutants. (A) All three proteins are homodimers in a candelabra configuration in which the helix−loop−helix monomers are connected by a disulfide bond in the loop region. (B−D) Mechanism of gaseous ligand biding. State B is the entatic state. (E) Sequences of HP7, the distal heme binding site knockout mutant HP7-H7F, and the entatic state stabilizing mutant CC9-H7F. Helices are underlined, and the b-position residues mutated in the transition from HP7 to CC9 are colored red. The positions in the heptad repeat sequence of each helix are annotated above the sequence comparison. H denotes a hydrophobic amino acid postion (●); P denotes a polar amino acid position (○).

in the future design of more complex artificial catalysts, to be able to effectively create high-affinity cofactor binding sites with controllable distal ligand affinity. It is therefore important to understand the factors that determine distal side chain affinity and its relationship to overall cofactor binding affinity.

MATERIALS AND METHODS

Chemicals. Oligonucleotides were purchased from Integrated DNA Technologies (Coralville, IA) and used without further purification. ^{15}N-labeled ammonium chloride was purchased from Cambridge Isotope Laboratories (Cambridge, MA). Pyocyanine was purchased from Cayman Chemical (Ann Arbor, MI). Hemin was purchased from Fluka (Buchs, Switzerland). All other solvents and reagents were from either Fisher Scientific or Sigma.

Cloning, Protein Expression, and Purification. The CC9 gene was synthesized (Biomatik Corp., Cambridge, ON) with an N-terminal TEV cut site and inserted between the BamHI and XhoI restriction sites of pET32a(+) (Novagen) as previously described.[12] Mutagenesis to produce CC9-H7F and HP7-H7F was accomplished using the Quikchange method (Stratagene Inc., La Jolla, CA). Mutagenized plasmid DNA was transformed into chemically competent *Escherichia coli* DH5α; the resulting clones were verified by sequencing, and a verified plasmid was transformed into BL21(DE3) cells for expression. Labeled and unlabeled proteins were expressed and purified as we have described previously.[12] Apoprotein concentrations were determined optically using an ε_{280} of 11.5 mM^{-1} cm^{-1} on the basis of their tryptophan content.[24]

Holoprotein complexes, containing 1.0 equiv per homodimer, were prepared as described previously[12] by five consecutive additions of 0.2 equiv of hemin in DMSO with at least 10 min between additions. Proteins were then purified from any unbound heme by being passed through a PD10 desalting columns pre-equilibrated with 250 mM boric acid and 100 mM KCl (pH 9.0). Holoprotein solution concentrations were determined using experimentally derived Soret ε_{414} values of 129 mM^{-1} cm^{-1} for HP7-H7F and 118 mM^{-1} cm^{-1} for CC9-H7F. If necessary, both holo- and apoproteins were concentrated using Centricon YM-10 spin concentrators (Millipore, Inc., Billerica, MA).

General Biochemistry. Optical spectra were recorded with a Hewlett-Packard (New York, NY) 8452A diode array spectrophotometer equipped with a Quantum Northwest (Liberty Lake, WA) Peltier temperature controller. Experiments requiring anaerobic conditions were conducted in an anaerobic cuvette[25] equipped with a platinum working and Red Rod (Radiometer Analytical, Lyon, France) reference electrode. All experiments were performed at 20 °C in 250 mM boric acid and 100 mM KCl (pH 9.0) unless otherwise noted. Each binding, reduction potential, and stopped-flow experiment was performed at least three times, and reported errors are standard deviations from the mean.

Circular Dichroism Spectropolarimetry. CD spectra were recorded on a JASCO J-810 sepectropolarimeter in a quartz cell with a 0.1 cm light path, using a bandwidth of 1 nm and a scan speed of 50 nm/min. HP7-H7F and CC9-H7F were prepared at concentrations of 24.15 and 14.75 μM, respectively, in 50 mM sodium phosphate (pH 7.5). Spectra were recorded between 190 and 280 nm, with background correction. The spectra were observed as ellipticity (θ_{obs}, millidegrees), and the mean residue ellipticity ($[\theta]$, degrees square centimeters per decimole) was calculated as

$$[\theta] = [\theta]_{obs}[MRW/(10lc)] \quad (1)$$

where MRW is the mean residue molecular weight, c is the sample concentration in milligrams per milliliter, and l is the light path length of the cell in centimeters. Protein secondary structure percentages were calculated with K2d[26] using data points ranging from 200 to 240 nm.

Stopped-Flow Analysis of Distal Histidine Dissociation. Binding kinetics of CO with the ferrous protein−heme complexes were followed spectroscopically in rapid stopped-flow mixing experiments over gas concentrations from 2 to 50% saturation at 15 °C using an Olis RSM 1000 spectrometer. Protein concentrations were 20−25 μM, and ferrous complexes were prepared by careful titration of anaerobic solutions of the holoproteins with a slight excess of dithionite as observed by visible spectroscopy and transferred to the stopped-flow loading syringe by canula. Binding kinetic data were fit with eq 2, which assumes that the CO binding rate, k_{+CO}, is much greater than the sum of the distal histidine association and dissociation

dx.doi.org/10.1021/bi201242a | *Biochemistry* 2011, 50, 10254−10261

rates:[9]

$$k_{obs} = \frac{k_{-H}k_{+CO}[CO]}{k_{+H} + k_{-H} + k_{+CO}[CO]} \quad (2)$$

where k_{obs} is the fitted single-exponential binding rate, k_{+H} and k_{-H} are the distal histidine−ferrous heme iron association and dissociation rates, respectively, and k_{+CO} is the CO association rate constant. This experiment determines the distal histidine ligand dissociation rate, at a high CO concentration ($k_{obs} = k_{-H}$).

Flash Photolysis Analysis of Distal Histidine Association. The rate constants for binding of both CO and histidine to the pentacoordinate state were determined using laser flash photolysis. A 1 ns pulse width frequency-doubled YAG laser at 532 nm excites the preformed carbonmonoxyferrous complex, causing the detachment of the ligand CO. This transiently forms an unliganded pentacoordinate heme protein, and the rates of these binding processes were determined by analyzing the multiexponential rebinding traces taken as a function of CO concentration using the method of Hargrove:[27]

$$\gamma_1 + \gamma_2 = k_{-H} + k_{+H} + k_{+CO}[CO] \quad (3)$$

$$\gamma_1\gamma_2 = k_{-H}k_{+CO}[CO] \quad (4)$$

where γ_1 and γ_2 are the fitted first and second CO-dependent exponential rates, respectively, and the kinetic constants are defined as in eq 1. Protein concentrations were 20−25 μM, and carbonmonoxyferrous complexes were prepared by titrating solutions of the holoproteins with an excess of dithionite as observed by visible spectroscopy under an atmosphere containing 10−100% CO mixed with argon.

Heme Affinity Measurements. Hemin stock solutions of approximately 0.5−1.0 mg/mL were prepared in DMSO and used within 6 h. Stock solution concentrations were determined using the pyridine hemochrome assay.[28] In oxidized binding experiments, 0.5−2 μL aliquots of a hemin solution, consisting of approximately 0.1 molar equiv, were added via gastight syringe to a stirring 4 mL solution of 2−3 μM protein, with a 10 min equilibration delay between additions. Heme binding was monitored by the loss of absorption at 385 nm due to free hemin, and the concomitant appearance of a sharp Soret band at 412 nm, corresponding to heme bound to the protein via bis-histidine axial coordination. The number of heme binding sites was quantified for each protein from plots of the Soret maximum at 412 nm versus the number of equivalents added.

For reduced binding experiments, 9.0 mL of ~3 μM protein was made anaerobic by extended flushing with nitrogen, and the solution potential was reduced to less than −450 mV versus NHE by the addition of a small volume (<20 μL) of sodium dithionite dissolved in degassed 100 mM KOH. The solution potential was monitored throughout the binding titration and kept below −450 mV by periodic additions of microliter volumes of sodium dithionite. Hemin was added in approximately 0.1 molar equiv aliquots with an at least 10 min equilibration period before spectra were recorded. K_d values were obtained from plots of the Soret band absorbance measured at 436 nm versus the concentration of hemin added and fit with the tight binding equation:

$$\Delta A = A_{start} + \varepsilon_{unb}[hem] + \varepsilon_{bnd}[prot] \times\left(\left\{K_d + [hem] + [prot] - \left[(K_d + [hem] + [prot])^2 - 4[hem][prot]\right]^{1/2}\right\}/(2[prot])\right) \quad (5)$$

where ε_{and} is the molar absorption coefficient of unbound hemin at that wavelength, ε_{bnd} is the additional absorbance of bound hemin at that wavelength, [hem] is the hemin concentration, [prot] is the protein concentration, and K_d is the dissociation constant for the reduced hemin.

Determination of Reduction Potentials. Redox titrations were performed in combination with optical analysis as described previously.[13] Concentrated solutions of hemoprotein prepared in advance were diluted to 20−30 μM into a solution containing the corresponding apoprotein (>100 μM) to eliminate the possibility of heme dissociation upon reduction. Reported reduction potentials are referenced to a standard hydrogen electrode. All redox titrations were performed anaerobically using microliters additions of freshly prepared sodium dithionite to adjust the solution potential to more negative values and potassium ferricyanide to more positive values. Redox titrations were analyzed by monitoring the absorbance bands at 559 and 425 nm as the heme protein was reduced or oxidized. The data were analyzed with the Nernst equation using an n value of 1.0:

$$\%R = \frac{1}{10^{(E-E_m)/[(RT)/(nF)]}} \quad (6)$$

where $\%R$ is the fraction of reduced heme, E is the solution potential, E_m is the reduction midpoint potential, and n is the number of electrons.

Nuclear Magnetic Resonance. All NMR experiments were performed at 20 °C on a Varian Inova spectrometer operating at a 600 MHz and equipped with a triple-resonance cryogenic probe capable of applying pulse field gradients in the z-direction. Data were processed using NMRPipe[29] and analyzed using Sparky.[30] For structural specificity assays, sensitivity-enhanced $^1H-^{15}N$ heteronuclear single-quantum coherence (HSQC) spectra[31] were recorded on 50−100 μM holo- and apoprotein samples with sweep widths of 10000 Hz for ^1H and 2000 Hz for ^{15}N utilizing GARP decoupling of ^{15}N during ^1H acquisition. Chemical shifts are referenced to water at 4.77 ppm for ^1H.

To determine the pK_a of histidine side chains, we collected imidazole $^1H-^{15}N$ multiple-bond correlation signals using a non-sensitivity-enhanced HSQC pulse sequence in which the INEPT (insensitive nuclei enhanced by polarization transfer) periods were set to $1/^1J_{NH}$, where $^1J_{NH}$ is the one-bond $^1H-^{15}N$ coupling constant, to attenuate backbone amide signals.[32,33] Spectral widths were 8000 Hz for ^1H and 12156 Hz for ^{15}N. Lyophilized ^{15}N-labeled apoprotein samples were dissolved in 25 mM KaD_2PO_4/D_2O buffer (pD 5.0) (pH meter reading + 0.4 pH unit); a spectrum was recorded, and the pD was adjusted upward by the addition of small amounts of KOD dissolved in D_2O. The observed ^{15}N chemical shifts were fit with the Henderson−Hasselbach equation:

$$\delta_{obs} = \frac{\Delta\delta_{prot}}{1 + 10^{pH-pK_a}} + \delta_0 \quad (7)$$

where δ_0 is the neutral chemical shift of ^{15}N, δ_{prot} is the change in chemical shift due to protonation, and pK_a is the fitted acid dissociation constant.

RESULTS AND DISCUSSION

Protein Design. To simplify our analysis, we removed one binding site by mutating the histidine on the first helix to a phenylalanine, creating the protein HP7-H7F (see Table 1).

Table 1. Characterization of the Two HP7 Variants

	$\lambda_{max\_oxidized}$ (mM^{-1} cm^{-1})	$\lambda_{max\_reduced}$ (mM^{-1} cm^{-1})	$\lambda[\theta]_{222}$ (deg cm^2 $dmol^{-1}$)	% α-helix
HP7-H7F	414 (129)	428 (140)	−8307	42
	530 (12.8)	532 (12.1)		
	558 (10.1)	560 (20.9)		
CC9-H7F	414 (118)	426 (139)	−15925	59
	530 (11.1)	530 (12.6)		
	556 (9.1)	560 (22.0)		

This protein retains the heme binding site nearest the connecting loops (Figure 1A). This is the opposite binding site that is occupied when the HP7 homodimer is bound to a single heme. To examine the thermodynamic effects of the buried charges, all three b-position glutamates on the second helix were mutated to alanine, which has both neutral hydrophobicity and high helical propensity.[34]

Both holoproteins display visible absorbance spectra indicative of bis-histidine coordination in both oxidation states (Figure 2A,C). It is important to confirm the helical bundle structure of each protein, as some designed helical bundle proteins have been found to form domain-swapped higher oligomeric states.[35] Both apo- and holoprotein forms of both HP7-H7F and CC9-H7F were single homodimers as analyzed by native gel electrophoresis in both the holo and apo states (data not shown). Circular dichroism spectra of the apo forms of both proteins demonstrate that both proteins are helical, with CC9-H7F having greater helical character. This is not surprising because each homodimer contains six mutations of glutamic acid to alanine, which has a significantly higher helical propensity.[36] Both had ^{15}N HSQC spectra indicative of molten globular structure (not shown). The addition of a single heme cofactor changes both spectra to a level of chemical shift dispersion indicative of a partial phase transition in which the two helices that ligate the heme become nativelike and the two unliganded helices remain molten globular, consistent with what we have previously observed for HP7.[12]

Oxidized Heme Binding. In the oxidized state, both proteins bind heme too tightly to reliably extract a dissociation constant even at protein concentrations as low as 200 nM. This has allowed us to perform end point titrations confirming that both proteins bind a single heme cofactor (Figure 2) and to calculate the extinction coefficient of the oxidized complex (Table 1).

Distal Histidine Affinity and the Histidine Dissociation Constant. To confirm that the triple mutation indeed stabilizes the affinity of the distal histidine, we must separately determine its association and dissociation rates. Figure 3A depicts the observed CO binding constants and their concentration dependence. For both proteins, CO binding to the ferrous state is monoexponential over more than five half-lives. Binding rates collected as a function of CO concentration demonstrate that CC9-H7F binds CO 22-fold more slowly than HP7-H7F (Table 2). As the protein is primarily in the hexacoordinate bis-histidine ligation state in solution (Figure 2), the rate-limiting step for CO binding at high ligand concentrations is thus the detachment of the distal histidine from the heme iron (see eq 2). Thus, histidine detachment is also 22-fold slower in CC9-H7F.

Distal Histidine Affinity and CO Flash Photolysis Determination of k_{+His}. Figure 3B depicts the rebinding kinetics of CO after laser-induced dissociation in CC9-H7F. In CC9-H7F, HP7-H7F, and our original analysis of HP7,[10] a fast exponential process that is independent of the concentration of CO is observed. Similar behavior has been observed in mouse neuroglobin and was ascribed to a relaxation process following a probable rearrangement caused by the change in heme iron planarity induced by detachment of the CO ligand.[37,38] In each case, two slower exponential processes, each of which varies in rate and magnitude with CO concentration, were also observed.

Replots of the sums and products of these two exponential processes are depicted in Figure 3C−F. The distal histidine binding rates are similar in both proteins, with the triple mutation slowing this process by a factor of 1.7 (Table 2). Combining these rates with the histidine off rates determined in the stopped flow experiments allows the calculation of the distal histidine affinity constants, K_A, for both proteins: −30 for

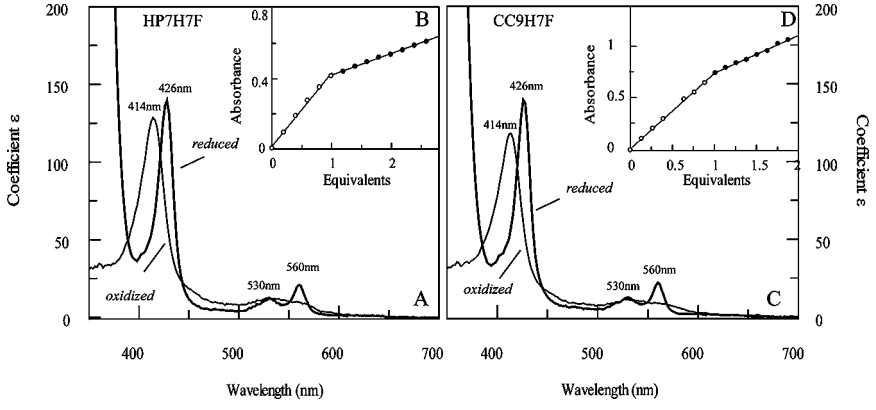

Figure 2. Absorption spectra and oxidized binding titrations of HP7-H7F and CC9-H7F with oxidized heme. (A) Oxidized and reduced spectra of heme-bound HP7-H7F. Extinction coefficients were calculated using the intercepts from the end point titrations in panel B. (C) Oxidized and reduced spectra of heme-bound CC9-H7F, calculated using the data from panel D.

dx.doi.org/10.1021/bi201242a | Biochemistry 2011, 50, 10254–10261

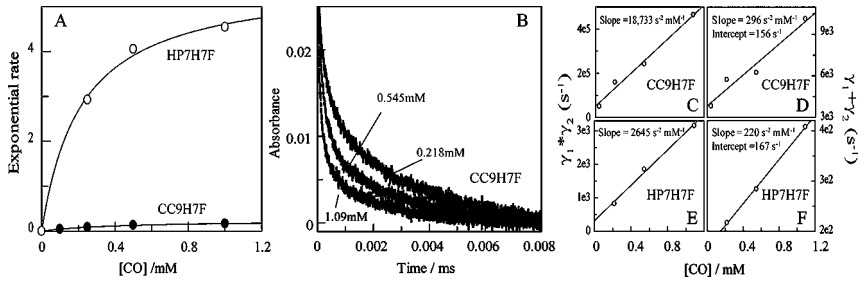

Figure 3. Kinetic analysis of CO and histidine binding to HP7-H7F and CC9-H7F. (A) Stopped-flow analysis of the rates of binding of CO to reduced heme proteins as a function of ligand concentration. Lines are fits with eq 1. (B) Laser flash kinetic analysis of histidine and CO rebinding to CC9-H7F followed at 419 nm. These data were fit with three exponentials, the first of which represents a CO concentration-independent relaxation process. (C–F) Replots of the sums and products of the second two exponentials.

Table 2. Thermodynamic Parameters for Two Artificial Heme Proteins

heme protein	$K_{d,red}$ (μM)	E_m (mV vs NHE)	$K_{d,ox}$ (nM)	pK_a	k_{-His} (s^{-1})	k_{+His} (s^{-1})	$K_{A,His}$	$K_{d,pent}$ (μM)
HP7-H7F	0.6 ± 0.2	−260 ± 6	0.3 ± 0.1	7.3 ± 0.2	160 ± 20	5.6 ± 0.3	29 ± 5	18 ± 9
CC9-H7F	2.9 ± 0.4	−195 ± 2	19 ± 3	6.39 ± 0.01	94 ± 11	0.25 ± 0.01	380 ± 60	1100 ± 300

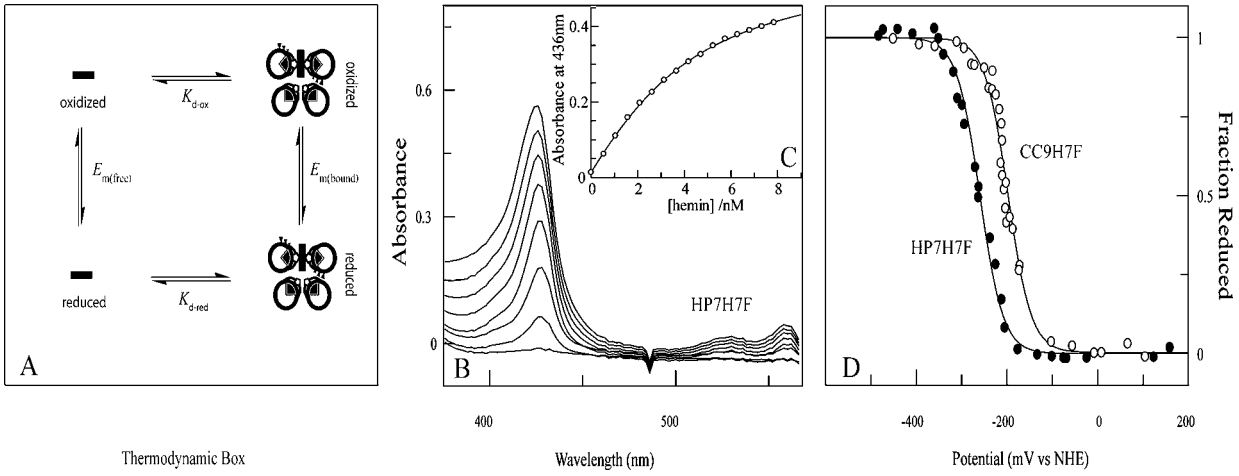

Figure 4. Thermodynamic cycle analysis of oxidized heme affinity. (A) Thermodynamic box used to determine $K_{d,ox}$. (B) Spectrometric titration of reduced heme binding to 3.0 μM HP7-H7F in 250 mM boric acid and 100 mM KCl (pH 9.0). Some spectra have been omitted for the sake of clarity. (C) Equilibrium binding isotherm derived from the titration in panel B. The line drawn is a fit with eq 4 using a $K_{d,red}$ of 600 nM. (D) Equilibrium potentiometric determination of the electron affinities of HP7-H7F and CC9-H7F. Lines are fits with eq 1.

HP7-H7F and 380 for CC9-H7F (as this is an intramolecular interaction, the association constant is dimensionless). Thus, the removal of the residues that were implanted to create the entatic state in HP7 stabilizes the hexacoordinate state in the ferrous protein by 1.5 kcal/mol.

Reduced Heme Binding. Gibney and co-workers have determined the solution reduction potential of an isolated heme cofactor, −63 mV versus the standard hydrogen electrode, using two different designed heme proteins and a thermodynamic cycle.[39] This value allows an alternate method for the determination of heme binding constants: experimentally determine the binding affinity in the reduced state, taking advantage of the weaker histidine–ferrous heme iron interaction,[40] and then calculation of the oxidized heme binding constant in combination with the bound and unbound heme reduction potentials using a similar thermodynamic cycle (see Figure 4A). Binding titrations conducted under reducing conditions give reproducible binding curves (see Figure 4B), and the fitted ferrous heme dissociation constants were 0.6 ± 0.2 μM for HP7-H7F and 2.6 ± 0.6 μM for CC9-H7F.

Reduction Potentials. The potentiometric analysis of the two proteins is depicted in Figure 4C. HP7-H7F, at −260 ± 6 mV versus NHE, has a reduction potential 65 mV lower than that of CC9-H7F (see Table 2) and 40 mV higher than that of the progenitor protein HP7 complexed with two hemes (−300 mV vs NHE[10]). HP7 rotates two sets of three glutamates into the core upon binding these two hemes. HP7-H7F rotates only one set of three, and CC9-H7F does not bury any charged residues in the core. Thus, each set of three buried glutamates imparts a change in reduction potential of approximately −50 mV, or 1.2 kcal/mol.

The reduction potentials, coupled with the reduced state affinities, allow the calculation of oxidized affinities of 300 ± 100 pM and 19 ± 3 nM for HP7-H7F and CC9-H7F, respectively. Given that the distal histidine binds more tightly to the heme iron in CC9-H7F than in HP7-H7F, the weaker energy of the former for heme binding is counterintuitive. This discrepancy might be explained by a large difference in bound cofactor reduction potentials, caused by some alteration in the local structure and/or electrostatics that moves the heme potential in the negative direction. The potentials, however,

move in the direction predicted by simple electrostatics (positive), and thus, the ferric heme binding energy difference between CC9-H7F and HP7-H7F is even larger.

NMR Titration of the Histidine pK_a. Histidine residues can be protonated, and the resultant histidine cation cannot bind heme. This proton competition effect is another possible explanation for the loss of binding affinity in the triple mutant protein.[39] To determine whether this is the case, NMR was used to determine the pK_a of the molten globular apoprotein histidine ligands. Both protein's histidine pK_a values were well below the solution pH (9.0) used in the binding titrations (Figure 5), with that of CC9-H7F approaching the solution pK_a

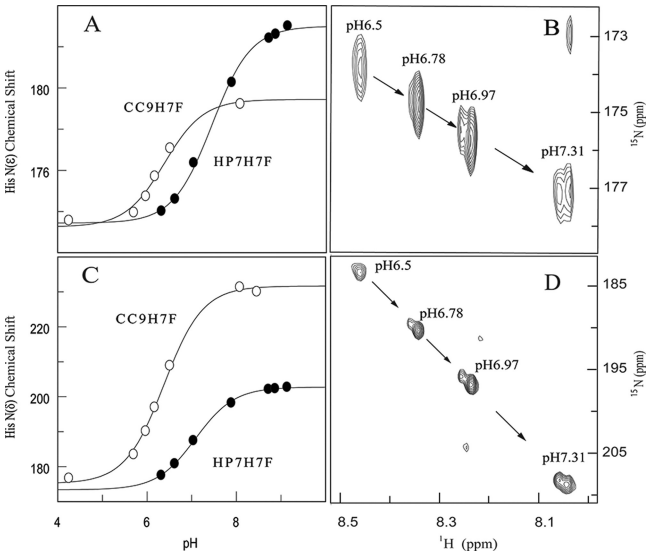

Figure 5. NMR determination of the pK_a values of the histidine ligands in apo-HP7-H7F and apo-CC9-H7F. (A) Fits of the $^{15}N^{\varepsilon 2}$ chemical shifts with eq 4. (B) Overlay of multiple-bond correlated $^1H-^{15}N$ spectra as a function of pH, showing the titration of the imidazole $H^{\varepsilon 1}-N^{\varepsilon 2}$ signals of histidine side chains. (C) Fits of the $^{15}N^{\delta 1}$ chemical shifts with eq 4. (D) Overlay of multiple-bond-correlated $H^{\varepsilon 1}-N^{\delta 1}$ signals of histidine side chains.

for free histidine; therefore, the observed differences in heme K_d are not a consequence of proton competition.

On the basis of the crystal[14] and NMR[41] structures of the progenitor protein BB in its apo form, the apoprotein forms of HP7-H7F and CC9-H7F can be expected to take a conformation in which the histidine side chains are buried in the protein core and the b-position residues exposed on the surface. Given this solvent exposure, it is not surprising that the removal of six negatively charged side chains has such a weak effect on the histidine pK_a. In the heme-bound state, however, b-position residues rotate into the low-dielectric hydrophobic core (Figure 1B) and electrostatic coupling has a larger effect, as demonstrated by the change in reduction potentials between the two proteins.

Origin of the Difference in Heme Affinities in the Two Proteins. Heme binding in hexacoordinate hemoglobins is a three-state process consisting of the apoprotein, a pentacoordinate bound state, and a hexacoordinate bound state (Figure 6A–C), with the latter two states considered bound states. Binding affinity in such a case was first examined by Morrison and co-workers in their analysis of slow, tight binding enzyme inhibition.[42] Extending this model to the hexacoordinate hemoglobins gives the relation

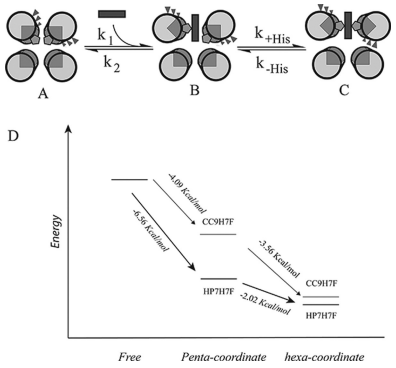

Figure 6. Comparative energy levels of the binding states of the two proteins. (A–C) Details of the binding mechanism. Heme binding initially occurs via a pentacoordinate encounter complex (B), which is followed by a protein conformational change driven by distal histidine attachment, resulting in the hexacoordinate, bis-histidine bound state (C). (D) Energy level diagram depicting the relative energies of each of these states in the two proteins. The absolute energies of the free states are unknown and are set equal to each other for comparative purposes.

$$K_d = \frac{k_2}{k_1}\left(\frac{k_{-His}}{k_{-His} + k_{+His}}\right) \quad (8)$$

where the ratio k_1/k_2 is $K_{d,pent}$, the dissociation constant that reflects the two-state energy difference between the apo state and the pentacoordinate state, and the term in parentheses represents the additional binding energy conferred by distal histidine ligation. Combining the experimental ferrous binding constant with the distal histidine ligation rate constants allows the calculation of $K_{d,pent}$ (Table 2).

These values explain the increase in the dissociation constant in CC9-H7F; $K_{d,pent}$ is increased by a factor of more than 60 by the triple mutation. An energy diagram that relates the relative energies of each of these states is depicted in Figure 6D. This graphically demonstrates that the increased affinity of the distal histidine incompletely compensates for the large loss of interaction energy of the pentacoordinate state. The structural origin of this loss in affinity is unclear. One possibility is that in the pentacoordinate state the b-position glutamate side chains on the helix with the distal (detached) histidine form van der Waals interactions with the bound heme, and the removal of these side chains therefore weakens the shape complementarity of the binding site. Another possibility is similar behavior in the helix containing the proximal (attached) histidine ligand. These differing possibilities point to the limitations inherent in the homodimeric candelabra scaffold. It may be that a single-chain protein,[43] which allows the independent optimization of each helix in a manner independent of the other, will allow both heme binding and distal histidine coordination to be optimized independently.

CONCLUSION

The detailed analysis presented here, of the effects of the mutational manipulation of the entatic state energy in an artificial oxygen transport protein, points to the difficulties inherent in the design and optimization of a functional protein with several conformational and oxidation states. Recent progress in the protein design field has made the creation of a natively structured, high-affinity ferric heme protein relatively straightforward, but functional proteins will necessarily require

dx.doi.org/10.1021/bi201242a | Biochemistry 2011, 50, 10254–10261

high cofactor affinity in, at the least, both the ferric and ferrous oxidation states of the heme cofactor. Early successes in the design of ferric heme binding proteins took advantage of the strong ferric iron−histidine interaction, estimated to be as high as 6 kcal/mol.[44] These interactions are much weaker, however, in the ferrous state,[40] and high-affinity binding of reduced heme and porphyrin cofactors in designed proteins will require a much more sophisticated combination of stabilizing interactions such as binding site complementarity, electrostatic pairing, and heme ligand rotamer optimization.[16,45]

AUTHOR INFORMATION

Corresponding Author

*E-mail: koder@sci.ccny.cuny.edu. Phone: (212) 650-5583.

Present Addresses

[§]Department of Biology, The Massachusetts Institute of Technology, Cambridge, MA 02139-4307.

[∥]School of Biochemistry, Medical Sciences Building, University of Bristol, Bristol, Avon BS8 1TD, U.K.

Funding

R.L.K. gratefully acknowledges support by the following grants: MCB-0920448 from the National Science Foundation (NSF), infrastructure support from P41 GM-66354 to the New York Structural Biology Center, and National Center for Research Resources Grant 5G12 RR03060 to The City College of New York. P.L.D. acknowledges equal support from NIH grant R01GM41048 and DOE BES grant DE FG02-ER0546223; P.L.D. and J.L.R.A. helped advise on experimental design to determine factors governing ferric and ferrous heme affinities and ligand binding dynamics and contributed toward development of synthetic protein structure/function design principles. I.A. and C.N. gratefully acknowledge support from the NIH's Minority Access to Research Careers program (T34 GM007639). A.C.M. gratefully acknowledges support from the Center for Exploitation of Nanostructures in Sensor and Energy Systems (CENSES) under NSF Cooperative Agreement Award 0833180. J.L.R.A. was supported by a Royal Society University Research Fellowship.

ACKNOWLEDGMENTS

We thank Brian Gibney (Department of Chemistry, Brooklyn College, Brooklyn, NY) and Mark Hargrove (Department of Biophysics, Iowa State University, Ames, IA) for many helpful discussions. We thank Hsin Wang (Department of Chemistry, The City College of New York) for assistance with NMR measurements.

ABBREVIATIONS

CO, carbon monoxide; HSQC, heteronuclear single-quantum coherence; NHE, normal hydrogen electrode.

REFERENCES

(1) Sheng, H., Yang, W., Fukuda, S., Tse, H. M., Paschen, W., Johnson, K., Batinic-Haberle, I., Crapo, J. D., Pearlstein, R. D., Piganelli, J., and Warner, D. S. (2009) Long-term neuroprotection from a potent redox-modulating metalloporphyrin in the rat. *Free Radical Biol. Med. 47*, 917−923.

(2) Koder, R. L., and Dutton, P. L. (2006) Intelligent design: The de novo engineering of proteins with specified functions. *Dalton Trans. 25*, 3045−3051.

(3) Lu, Y. (2005) Design and engineering of metalloproteins containing unnatural amino acids or non-native metal-containing cofactors. *Curr. Opin. Chem. Biol. 9*, 118−126.

(4) Robertson, D. E., Farid, R. S., Moser, C. C., Urbauer, J. L., Mulholland, S. E., Pidikiti, R., Lear, J. D., Wand, A. J., Degrado, W. F., and Dutton, P. L. (1994) Design and Synthesis of Multi-Heme Proteins. *Nature 368*, 425−431.

(5) Choma, C. T., Lear, J. D., Nelson, M. J., Dutton, P. L., Robertson, D. E., and Degrado, W. F. (1994) Design of a Heme-Binding 4-Helix Bundle. *J. Am. Chem. Soc. 116*, 856−865.

(6) Cowley, A. B., Kennedy, M. L., Silchenko, S., Lukat-Rodgers, G. S., Rodgers, K. R., and Benson, D. R. (2006) Insight into heme protein redox potential control and functional aspects of six-coordinate ligand-sensing heme proteins from studies of synthetic heme peptides. *Inorg. Chem. 45*, 9985−10001.

(7) Reedy, C. J., and Gibney, B. R. (2004) Heme protein assemblies. *Chem. Rev. 104*, 617−649.

(8) Cowley, A. B., and Benson, D. R. (2007) Weak-field anions displace the histidine ligand in a synthetic heme peptide but not in N-acetylmicroperoxidase-8: Possible role of heme geometry differences. *Inorg. Chem. 46*, 48−59.

(9) Trent, J. T., Hvitved, A. N., and Hargrove, M. S. (2001) A model for ligand binding to hexacoordinate hemoglobins. *Biochemistry 40*, 6155−6163.

(10) Koder, R. L., Anderson, J. L. R., Solomon, L. A., Reddy, K. S., Moser, C. C., and Dutton, P. L. (2009) Design and engineering of an O_2 transport protein. *Nature 458*, 305−309.

(11) Anderson, J. L. R., Koder, R. L., Moser, C. C., and Dutton, P. L. (2008) Controlling complexity and water penetration in functional de novo protein design. *Biochem. Soc. Trans. 36*, 1106−1111.

(12) Koder, R. L., Valentine, K. G., Cerda, J. F., Noy, D., Smith, K. M., Wand, A. J., and Dutton, P. L. (2006) Native-like structure in designed four helix bundles driven by buried polar interactions. *J. Am. Chem. Soc. 128*, 14450−14451.

(13) Huang, S. S., Koder, R. L., Lewis, M., Wand, A. J., and Dutton, P. L. (2004) The HP-1 maquette: From an apoprotein structure to a structured hemoprotein designed to promote redox-coupled proton exchange. *Proc. Natl. Acad. Sci. U.S.A. 101*, 5536−5541.

(14) Huang, S. S., Gibney, B. R., Stayrook, S. E., Dutton, P. L., and Lewis, M. (2003) X-ray Structure of a Maquette Scaffold. *J. Mol. Biol. 326*, 1219−1225.

(15) Discher, B. M., Koder, R. L., Moser, C. C., and Dutton, P. L. (2003) Hydrophilic to Amphiphilic Design in Redox Protein Maquettes. *Curr. Opin. Chem. Biol. 7*, 741−748.

(16) Negron, C., Fufezan, C., and Koder, R. L. (2009) Helical Templates for Porphyrin Binding in Designed Proteins. *Proteins: Struct., Funct., Bioinf. 74*, 400−416.

(17) Hecht, M. H., Das, A., Go, A., Bradley, L. H., and Wei, Y. N. (2004) De novo proteins from designed combinatorial libraries. *Protein Sci. 13*, 1711−1723.

(18) Kamtekar, S., Schiffer, J. M., Xiong, H. Y., Babik, J. M., and Hecht, M. H. (1993) Protein Design by Binary Patterning of Polar and Nonpolar Amino-Acids. *Science 262*, 1680−1685.

(19) Moffet, D. A., and Hecht, M. H. (2001) De novo proteins from combinatorial libraries. *Chem. Rev. 101*, 3191−3203.

(20) Wei, Y. N., Kim, S., Fela, D., Baum, J., and Hecht, M. H. (2003) Solution structure of a de novo protein from a designed combinatorial library. *Proc. Natl. Acad. Sci. U.S.A. 100*, 13270−13273.

(21) Wei, Y. N., Liu, T., Sazinsky, S. L., Moffet, D. A., Pelczer, I., and Hecht, M. H. (2003) Stably folded de novo proteins from a designed combinatorial library. *Protein Sci. 12*, 92−102.

(22) Vallee, B. L., and Williams, R. J. P. (1968) Metalloenzymes: Entatic nature of their active sites. *Proc. Natl. Acad. Sci. U.S.A. 59*, 498.

(23) Brunori, M., Giuffre, A., and Sarti, P. (2005) Cytochrome c oxidase, ligands and electrons. *J. Inorg. Biochem. 99*, 324−336.

(24) Pace, C. N., Vajdos, F., Fee, L., Grimsley, G., and Gray, T. (1995) How to Measure and Predict the Molar Absorption Coefficient of a Protein. *Protein Sci. 4*, 2411−2423.

(25) Dutton, P. L. (1978) Redox potentiometry: Determination of midpoint potentials of oxidation-reduction components of biological electron-transfer systems. *Methods Enzymol. 54*, 411−435.

(26) Andrade, M. A., Chacon, P., Merelo, J. J., and Moran, F. (1993) Evaluation of secondary structure of proteins from UV circular-dichroism spectra using an unsupervised learning neural network. *Protein Eng. 6*, 383−390.
(27) Hargrove, M. S. (2000) A flash photolysis method to characterize hexacoordinate hemoglobin kinetics. *Biophys. J. 79*, 2733−2738.
(28) Berry, E. A., and Trumpower, B. L. (1987) Simultaneous determination of hemes-A, hemes-B, and hemes-C from pyridine hemochrome spectra. *Anal. Biochem. 161*, 1−15.
(29) Delaglio, F., Grzesiek, S., Vuister, G., Zhu, G., Pfeifer, J., and Bax, A. (1995) NMRPipe: A Multidimensional Spectral Processing System Based on UNIX Pipes. *J. Biomol. NMR 6*, 277−293.
(30) Goddard, T. D., and Kneller, D. G. (2007) *Sparky*, University of California, San Francisco.
(31) Kay, L. E., Keifer, P., and Saarinen, T. (1992) Pure Absorption Gradient Enhanced Heteronuclear Single Quantum Correlation Spectroscopy with Improved Sensitivity. *J. Am. Chem. Soc. 114*, 10663−10665.
(32) Pelton, J. G., Torchia, D. A., Meadow, N. D., and Roseman, S. (1993) Tautomeric states of the active-site histidines of phosphorylated and unphosphorylated III(GLC), a signal-transducing protein from *Escherichia coli*, using 2-dimensional heteronuclear NMR techniques. *Protein Sci. 2*, 543−558.
(33) Nanda, V., and Koder, R. L. (2010) Designing artificial enzymes by intuition and computation. *Nat. Chem. 2*, 15−24.
(34) Lyu, P. C., Liff, M. I., Marky, L. A., and Kallenbach, N. R. (1990) Side-Chain Contributions to the Stability of α-Helical Structure in Peptides. *Science 250*, 669−673.
(35) Ogihara, N. L., Ghirlanda, G., Bryson, J. W., Gingery, M., DeGrado, W. F., and Eisenberg, D. (2001) Design of three-dimensional domain-swapped dimers and fibrous oligomers. *Proc. Natl. Acad. Sci. U.S.A. 98*, 1404−1409.
(36) Dunbrack, R. L., and Karplus, M. (1993) Backbone-Dependent Rotamer Library for Proteins: Application to Side-Chain Prediction. *J. Mol. Biol. 230*, 543−574.
(37) Ascenzi, P., Bocedi, A., de Sanctis, D., Pesce, A., Bolognesi, M., Marden, M. C., Dewilde, S., Moens, L., Hankeln, T., and Burmester, T. (2004) Neuroglobin and cytoglobin: Two new entries in the hemoglobin superfamily. *Biochem. Mol. Biol. Educ. 32*, 305−313.
(38) Du, W. H., Syvitski, R., Dewilde, S., Moens, L., and La Mar, G. N. (2003) Solution ^{1}H NMR characterization of equilibrium heme orientational disorder with functional consequences in mouse neuroglobin. *J. Am. Chem. Soc. 125*, 8080−8081.
(39) Reddi, A. R., Reedy, C. J., Mui, S., and Gibney, B. R. (2007) Thermodynamic investigation into the mechanisms of proton-coupled electron transfer events in heme protein maquettes. *Biochemistry 46*, 291−305.
(40) Reedy, C. J., Kennedy, M. L., and Gibney, B. R. (2003) Thermodynamic characterization of ferric and ferrous haem binding to a designed four-α-helix protein. *Chem. Commun.*, 570−571.
(41) Skalicky, J. J., Gibney, B. R., Rabanal, F., Urbauer, R. J. B., Dutton, P. L., and Wand, A. J. (1999) Solution structure of a designed four-α-helix bundle maquette scaffold. *J. Am. Chem. Soc. 121*, 4941−4951.
(42) Sculley, M. J., and Morrison, J. F. (1986) The determination of kinetic constants governing the slow,tight-binding inhibition of enzyme-catalyzed reactions. *Biochim. Biophys. Acta 874*, 44−53.
(43) Bender, G. M., Lehmann, A., Zou, H., Cheng, H., Fry, H. C., Engel, D., Therien, M. J., Blasie, J. K., Roder, H., Saven, J. G., and DeGrado, W. F. (2007) De novo design of a single-chain diphenylporphyrin metalloprotein. *J. Am. Chem. Soc. 129*, 10732−10740.
(44) Shifman, J. M., Moser, C. C., Kalsbeck, W. A., Bocian, D. F., and Dutton, P. L. (1998) Functionalized de novo designed proteins: Mechanism of proton coupling to oxidation/reduction in heme protein maquettes. *Biochemistry 37*, 16815−16827.
(45) Braun, P., Goldberg, E., Negron, C., von Jan, M., Xu, F., Nanda, V., Koder, R. L., and Noy, D. (2011) Design principles for chlorophyll-binding sites in helical proteins. *Proteins: Struct., Funct., Bioinf. 79*, 463−476.